LETTER

doi:10.1038/nature11317

Human ES-cell-derived cardiomyocytes electrically couple and suppress arrhythmias in injured hearts

Yuji Shiba[1,2]*, Sarah Fernandes[1]*, Wei-Zhong Zhu[1], Dominic Filice[1,3], Veronica Muskheli[1], Jonathan Kim[1], Nathan J. Palpant[1], Jay Gantz[1,3], Kara White Moyes[1], Hans Reinecke[1], Benjamin Van Biber[1], Todd Dardas[4], John L. Mignone[4], Atsushi Izawa[2], Ramy Hanna[4], Mohan Viswanathan[4], Joseph D. Gold[5], Michael I. Kotlikoff[6], Narine Sarvazyan[7], Matthew W. Kay[7,8], Charles E. Murry[1,3,4] & Michael A. Laflamme[1]

Transplantation studies in mice and rats have shown that human embryonic-stem-cell-derived cardiomyocytes (hESC-CMs) can improve the function of infarcted hearts[1–3], but two critical issues related to their electrophysiological behaviour *in vivo* remain unresolved. First, the risk of arrhythmias following hESC-CM transplantation in injured hearts has not been determined. Second, the electromechanical integration of hESC-CMs in injured hearts has not been demonstrated, so it is unclear whether these cells improve contractile function directly through addition of new force-generating units. Here we use a guinea-pig model to show that hESC-CM grafts in injured hearts protect against arrhythmias and can contract synchronously with host muscle. Injured hearts with hESC-CM grafts show improved mechanical function and a significantly reduced incidence of both spontaneous and induced ventricular tachycardia. To assess the activity of hESC-CM grafts *in vivo*, we transplanted hESC-CMs expressing the genetically encoded calcium sensor, GCaMP3 (refs 4, 5). By correlating the GCaMP3 fluorescent signal with the host ECG, we found that grafts in uninjured hearts have consistent 1:1 host–graft coupling. Grafts in injured hearts are more heterogeneous and typically include both coupled and uncoupled regions. Thus, human myocardial grafts meet physiological criteria for true heart regeneration, providing support for the continued development of hESC-based cardiac therapies for both mechanical and electrical repair.

Although hESC-CMs form gap junctions and beat synchronously *in vitro*[6,7], there is only indirect evidence for their electromechanical integration after transplantation[6–8]. We do not know whether hESC-CM grafts contract synchronously at physiological human rates, integrate in injured hearts despite scar tissue, or affect electrical stability. Indeed, both pro-arrhythmic[9] and anti-arrhythmic[10] effects have been reported for mouse cardiomyocyte grafts in injured mouse hearts. Human cardiac grafts could plausibly contribute to arrhythmogenesis through automaticity[11–14] and triggered activity[15], and their irregular graft geometry could promote reentry[1–3,16].

To address these uncertainties, we employed a new guinea-pig model of cardiac injury. Prior work with hESC-CMs in infarcted hearts was carried out in mice and rats[1–3], but these species' rapid heart rates (approximately 600 and 400 beats per minute (b.p.m.), respectively[17]) may prevent host–graft coupling or arrhythmias that could occur in humans. *In vitro* hESC-CMs show a spontaneous rate of approximately 50 to 150 b.p.m.[12,13,18] and can be paced up to 240 b.p.m., suggesting that they can keep up with the guinea-pig heart (approximately 200 to 250 b.p.m.[19]).

We first examined the structural, mechanical and electrocardiographic consequences of hESC-CM transplantation in injured hearts of immunosuppressed guinea-pigs (Supplementary Fig. 1a). hESC-CMs were derived from H7 hESCs, as previously described[2,20]. Adult guinea-pigs were subjected to cardiac cryoinjury and implanted with telemetric electrocardiographic (ECG) transmitters. Ten days later, they underwent a repeat thoracotomy and intra-cardiac injection of either 1×10^8 hESC-CMs in a pro-survival cocktail (PSC) of factors previously shown to enhance hESC-CM engraftment[2] ($n = 15$), 1×10^8 non-cardiac hESC-derivatives in PSC (non-CMs; $n = 13$), or PSC vehicle alone ($n = 14$). hESC-CMs were 63% pure by anti-α-actinin flow cytometry, whereas non-CMs included no detectable cardiomyocytes (Supplementary Fig. 2).

Twenty-eight days after transplantation, all animals showed transmural scar and thinning of the left ventricle. Scar area was not different among the groups (13.2 ± 0.9% of the left ventricle in hESC-CM, 14.8 ± 1.4% in non-CM, and 15.3 ± 1.9% in PSC-only recipients). However, hESC-CM recipients showed partial remuscularization with islands of human myocardium occupying 8.4 ± 1.5% of the scar area (Fig. 1a). The human origin of these grafts was confirmed by *in situ* hybridization with a human pan-centromeric probe, and more than 99% of the human cells immunostained positively with the cardiac marker β-myosin heavy chain (βMHC; also known as MYH7) (Fig. 1b and Supplementary Fig. 3a–f). No teratomas developed, and hESC-CM grafts were negative for multiple non-cardiac markers (Supplementary Fig. 3g–k). Most of the graft myocardium was located in the central scar, but there were occasional points of host–graft contact in the border zone with shared intercalated discs identified by anti-connexin 43 and cadherin immunostaining (Fig. 1c–h and Supplementary Fig. 3d, e). Minimal immune reaction was observed in sections stained with a guinea-pig-specific pan-leukocyte marker (Supplementary Fig. 3l). Grafts were supplied by host-derived neovessels that contained erythrocytes, indicating perfusion by the host coronary circulation (Supplementary Fig. 3h, m–o).

Surviving human cells were found in only 7 of 13 non-CM recipients at 28 days after transplantation, and these grafts were smaller than those in hESC-CM recipients (less than 1% of the scar area). No βMHC-positive graft was detected in non-CM recipients; instead, the surviving human cells consisted of small epithelial nests and scattered fibroblastic cells (Supplementary Fig. 4).

Hearts receiving hESC-CMs, non-CMs and PSC only, were assessed by echocardiography on days −2 and +28 relative to cell transplantation. All groups showed increased left-ventricle dimensions and reduced fractional shortening on day −2 relative to uninjured controls

[1]Department of Pathology, Center for Cardiovascular Biology, Institute for Stem Cell and Regenerative Medicine, University of Washington, 850 Republican Street, Seattle, Washington 98109, USA. [2]Department of Cardiovascular Medicine, Shinshu University, 3-1-1 Asahi, Matsumoto, Nagano 390-8621, Japan. [3]Department of Bioengineering, Center for Cardiovascular Biology, Institute for Stem Cell and Regenerative Medicine, University of Washington, 850 Republican Street, Seattle, Washington 98109, USA. [4]Department of Medicine and Cardiology, Center for Cardiovascular Biology, Institute for Stem Cell and Regenerative Medicine, University of Washington, 1959 NE Pacific Street, Seattle, Washington 98195, USA. [5]Geron Corporation, 230 Constitution Drive, Menlo Park, California 94025 USA. [6]Department of Biomedical Sciences, College of Veterinary Medicine, Cornell University, Ithaca, New York 14853, USA. [7]Department of Pharmacology and Physiology, The George Washington University, 2300 I Street NW, Washington DC 20037 USA. [8]Department of Electrical and Computer Engineering, The George Washington University, 2300 I Street NW, Washington DC 20037 USA.
*These authors contributed equally to this work.

©2012 Macmillan Publishers Limited. All rights reserved

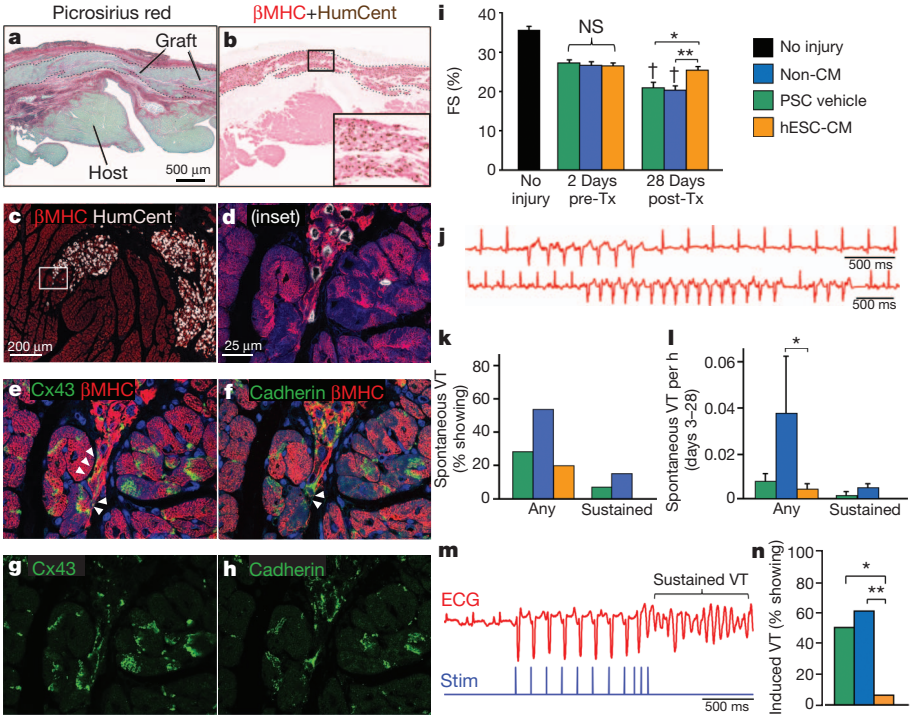

Figure 1 | Transplanted hESC-CMs partially remuscularize injured guinea-pig hearts, preserve mechanical function and reduce arrhythmia susceptibility. **a**, **b**, Twenty-eight-day-old hESC-CM grafts in a cryoinjured heart stained with picrosirius red (**a**), and anti-β-myosin heavy chain (βMHC, red) plus human-specific *in situ* probe (HumCent, brown) (**b**). **c**–**h**, Confocal image of host–graft contact, dual-labelled for HumCent (white) and βMHC (red) (**c**; a higher magnification image of the area in the white box in **c** is shown in **d**), de-stained and then immunostained for βMHC (red) and either connexin 43 (Cx43, green; **e** and **g**) or cadherins (green; **f** and **h**). Arrows indicate Cx43 and cadherin shared between graft and host myocytes. **i**, Left-ventricle fractional shortening (FS) by echocardiography in uninjured animals and cryoinjured recipients of PSC vehicle only, non-CMs or hESC-CMs at 2 days prior to and 28 days after transplantation (Tx). **j**, Representative telemetric ECGs, including non-sustained ventricular tachycardia (VT) in an hESC-CM recipient (top trace), as well as sustained VT and triplet PVCs in a non-CM recipient (bottom trace). **k**, Percentage of animals by group that showed spontaneous VT during monitoring from days 3 to 28 after transplantation. **l**, Frequency of spontaneous VT by group. **m**, ECG (red) and stimulation (blue) traces from a cryoinjured non-CM recipient induced to sustained VT by PES. **n**, Percentage of animals in each group induced to VT. All data are presented as mean ± s.e.m.; $n \geq 13$ per group. NS, not significant. $^{*}P < 0.05$; $^{**}P < 0.01$. †$P < 0.05$ versus day −2.

($n = 11$), but there were no differences among the cryoinjured groups (Fig. 1i and Supplementary Fig. 5). The two control groups exhibited further left ventricle dilation and deterioration of fractional shortening between days −2 and +28 ($P < 0.05$ for all pairwise comparisons between time points). This deterioration was completely attenuated in cryoinjured hESC-CM recipients, which showed significantly greater fractional shortening on day +28 than cryoinjured PSC-only or non-CM recipients ($P < 0.05$ and $P < 0.01$, respectively) (Fig. 1i).

Ambulatory telemetric ECG recordings were obtained regularly from 1 day after injury to 28 days after transplantation. Pilot studies revealed only rare premature ventricular contractions (PVCs) in uninjured animals, whereas cryoinjured but not transplanted animals showed occasional PVCs and runs of ventricular tachycardia (Supplementary Table 1). Interestingly, the hESC-CM group had the lowest fraction of animals with PVCs after transplantation and the lowest rate of couplet PVCs per hour (Supplementary Fig. 6). Moreover, fewer hESC-CM recipients showed spontaneous ventricular tachycardia, and hESC-CM recipients were the only group with no sustained ventricular tachycardia (Fig. 1j, k). Next, we counted all episodes of ventricular tachycardia from day 3 to 28 and found that non-CM recipients showed 785% more ventricular tachycardia episodes than hESC-CM recipients (95% confidence interval: 74% to +4,370%, $P < 0.01$; Fig. 1l).

As a final test of electrical stability, we induced arrhythmias through programmed electrical stimulation (PES). To detect either a positive or negative effect of cell transplantation, we developed a PES protocol that induced ventricular tachycardia in 40% of non-transplanted animals at 38 days after cryoinjury ($n = 5$), but not in uninjured animals ($n = 8$). When cryoinjured hESC-CM recipients were challenged with PES at 28 days after transplantation, ventricular tachycardia was induced in only 6.7% of these animals versus 61.5% and 50% of cryoinjured non-CM and PSC-only recipients, respectively ($P < 0.01$ by Fisher's exact test, Fig. 1m, n).

To explore the mechanism by which hESC-CMs improved mechanical and electrical function, we investigated whether the grafts were coupled and beat synchronously with host myocardium. We used zinc-finger nuclease (ZFN)-mediated transgenesis[21] to create hESC-CMs that stably expressed the genetically encoded fluorescent calcium sensor, GCaMP3 (refs 4, 5), and these myocytes exhibited robust fluorescence transients with each contractile cycle *in vitro* (Supplementary Fig. 7 and Supplementary Movie 1). We transplanted 1×10^8 GCaMP3-positive hESC-CMs (cardiac purity of 74 ± 10%) into intact and cryoinjured guinea-pig hearts and carried out intravital imaging at 2 or 4 weeks after transplantation (Supplementary Fig. 1b). Epicardial fluorescent transients indicated activation of the graft *in vivo*, and these were correlated with the ECG to determine their synchrony with host myocardium[10].

The GCaMP3-positive hESC-CM grafts in uninjured hearts had extensive host–graft contact with little intervening fibrosis (Fig. 2a and Supplementary Fig. 8a). Correspondingly, these hearts showed an impressive degree of host–graft electromechanical integration. We found large GCaMP3-positive hESC-CMs grafts in all uninjured recipients at 14 days after transplantation ($n = 9$), and 100% of the visible graft in each animal showed calcium fluorescence transients that synchronized 1:1 with systole in the host ECG (Fig. 2b). These hearts were also imaged *ex vivo* during mechanical arrest with either 2,3-butanedione monoxime (BDM) or blebbistatin ($n = 11$). 1:1 host–graft coupling continued under these conditions, ruling out confounding motion artefacts and the possibility of indirect graft activation by passive stretch (Supplementary Fig. 8 b, c and Supplementary Movie 2). hESC-CM grafts in uninjured hearts remained fully coupled during pacing at rates ≥5 Hz (Fig. 2c).

Next, we transplanted GCaMP3-positive hESC-CMs at 10 days after cryoinjury and carried out intravital imaging at 14 and 28 days after transplantation ($n = 7$ and $n = 15$ animals, respectively). By histology, surviving grafts at both time points were mostly located within the central scar, although occasional points of host–graft contact in the border zone were identified (Fig. 3a and Supplementary Fig. 9a). Dual labelling with a guinea-pig-specific *in situ* probe and anti-green fluorescent protein (GFP) immunostaining ruled out a meaningful

©2012 Macmillan Publishers Limited. All rights reserved

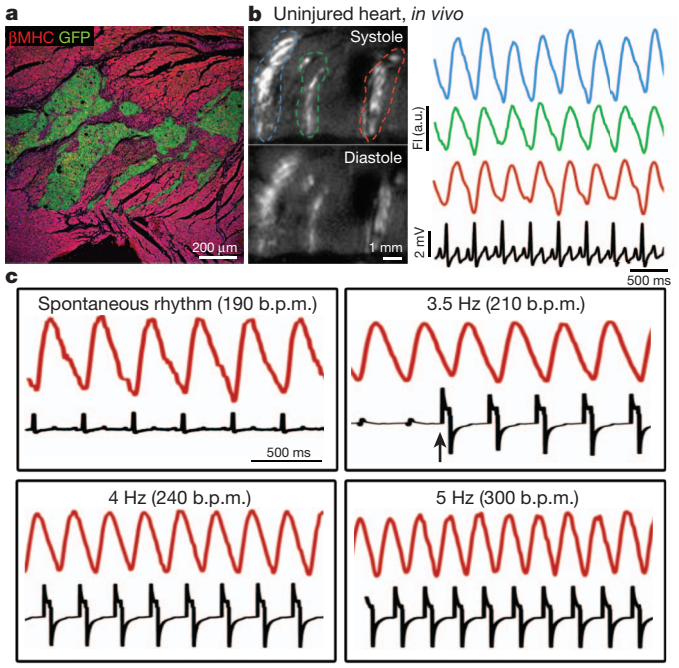

Figure 2 | hESC-CM grafts in uninjured hearts show 1:1 coupling with host myocardium. **a**, GCaMP3-positive hESC-CM graft in an uninjured heart immunostained for GFP (green) and βMHC (red), showing extensive host–graft contact with minimal intervening scar. **b**, Left, GCaMP3-positive hESC-CM graft in an uninjured heart during systole and diastole, acquired using an open-chest preparation at 14 days after transplantation. Right, GCaMP3 fluorescence intensity (FI) versus time for the red, green and blue regions of interest indicated in the left panel, as well as the host ECG (black). GCaMP3 fluorescent transients in all three regions occurred with 1:1 coupling with QRS complexes of the host ECG. a.u. arbitrary units. **c**, GCaMP3 fluorescent signal (red) and ECG (black) from a representative hESC-CM graft in an uninjured heart, imaged *ex vivo* under mechanical arrest. 1:1 host–graft coupling occurred during spontaneous beating and pacing at rates ≤5 Hz. Arrow, onset of pacing.

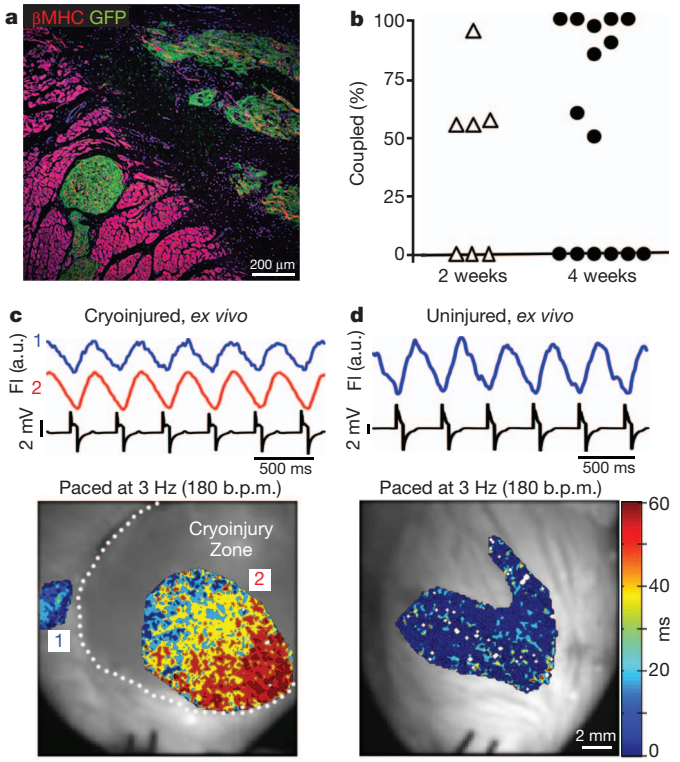

Figure 3 | hESC-CM grafts show 1:1 host–graft coupling in the majority of injured recipient hearts, but the extent of coupling and pattern of activation is variable. **a**, GCaMP3-positive hESC-CM graft in a cryoinjured heart immunostained for GFP (green) and βMHC (red). Small graft nests were located in host muscle within the border zone, but most of the graft was in scar. **b**, Percentage of visible GCaMP3-positive hESC-CM graft in each cryoinjured heart that showed 1:1 host–graft coupling at 14 and 28 days after transplantation ($n = 7$ and $n = 15$ animals, respectively). **c**, Representative 28-day-old GCaMP3-positive hESC-CM graft in a cryoinjured heart imaged *ex vivo* during mechanical arrest with blebbistatin and pacing at 3 Hz. Top, traces of mean fluorescent intensity versus time for graft regions located within host muscle (1, blue font) and the cryoinjury zone (2, red font). Both were activated in a 1:1 correlation with the host ECG (black). Bottom, corresponding activation map showing the interval (in ms) between the stimulus pulse and the local rise in GCaMP3 fluorescence. Graft in host muscle (1) showed uniformly rapid activation, whereas the graft in the scar (2) activated first in centre of the scar and then gradually progressed towards the border zone. On other occasions, graft activation started at the border zone and radiated into the scar. **d**, Top, traces of GCaMP3 fluorescence and EGG. Bottom, the activation map for a representative GCaMP3-positive hESC-CM graft in a blebbistatin-arrested uninjured heart. This graft showed 1:1 host–graft coupling and a brief interval between stimulus and GCaMP3 transient upstroke.

contribution of cell fusion to the observed GCaMP3 signals (Supplementary Fig. 9b and Supplementary Movie 3).

Cryoinjured hearts with GCaMP3-positive hESC-CM grafts showed robust epicardial fluorescence transients, but their behaviour was more heterogeneous than that of grafts in uninjured animals, with greater variation in size, distribution and temporal relationship to the host ECG. Given this complicated behaviour, we focused on imaging mechanically arrested hearts *ex vivo*, so that the grafts could be more completely visualized and the proportion of coupled and uncoupled graft could be quantified better (Supplementary Movies 4 and 5). We found regions of GCaMP3-positive graft with consistent 1:1 host–graft coupling in approximately 60% of hearts at both 14 and 28 days after transplantation (4 out of 7 animals, and 9 out of 15 animals, respectively; Fig. 3b and Supplementary Tables 2 and 3). Although there was no significant difference in the fraction of animals with coupled grafts between the two time points, in the subset of animals with at least some coupling, there was a trend towards greater host–graft coupling over time (66 ± 10% versus 87 ± 6% of visible graft at 14 and 28 days, respectively). No grafts with intermittent or partial coupling (for example, 1:2 or 1:3 host–graft coupling) were observed. Uncoupled graft regions showed regular GCaMP3 fluorescent transients, but these occurred with a periodicity unrelated to the ECG or neighbouring graft domains, usually at a rate slower than the host (at 28 days, 96 ± 11 b.p.m. versus a host rate of 176 ± 9 b.p.m.). By marking the coupled and non-coupled graft regions with indelible inks that survive histological processing, we found many examples of reliably coupled graft located within the central scar region, proving that coupling is not limited to grafts at the border zone (data not shown). When injured hearts with GCaMP3-positive hESC-CM grafts were paced, most of the initially coupled graft regions remained coupled up to 4 Hz, after which some loss of coupling was observed (Supplementary Fig. 10).

We next attempted to perform voltage mapping of graft and host myocardium in cryoinjured hearts but, unexpectedly, hESC-CM grafts failed to label with the potentiometric dyes RH237 and di-4-ANEPPS (Supplementary Fig. 11). hESC-CMs were readily labelled *in vitro* (Supplementary Fig. 12), so their poor staining *in vivo* probably reflects sluggish perfusion of the graft tissue and perhaps reduced membrane staining because of undeveloped T-tubules[22]. However, we did obtain good labelling of host myocardium with RH237 and we therefore compared voltage maps from cryoinjured hearts with and without grafts ($n = 6$ and $n = 4$ animals, respectively). As expected, both groups showed robust propagation in uninjured myocardium, whereas optical action potential amplitudes and epicardial conduction velocities were reduced in the cryoinjury zone. The two groups showed no significant differences in the amplitudes of optical action potentials within the injured zone or the kinetics of activation and repolarization

©2012 Macmillan Publishers Limited. All rights reserved

(Supplementary Figs 13 and 14), suggesting that hESC-CM transplantation does not exert major paracrine effects on host electrical behaviour.

Because the electrical activity of hESC-CM grafts could not be evaluated with potentiometric dyes, we used instead the GCaMP3 signal to assess graft activation and propagation. GCaMP3 transients lag depolarization owing to slow binding of calcium, but this delay should be the same throughout the graft[10,23], so graft activation maps can be generated using the time interval between electrical stimulation (or host QRS complex of the ECG) and the GCaMP3 transient. This revealed a marked difference in activation between grafts located in viable host muscle versus those in scar tissue (Fig. 3c, d). Grafts in intact myocardium were activated uniformly and within approximately 10 ms, probably reflecting synchronous activation through multiple points of contact with the host. In contrast, graft activation within scar tissue was spatially and temporally heterogeneous, even in regions with 1:1 coupling. These coupled grafts showed initial activation within approximately 10 to 20 ms, but the spread of activation was slower, such that some areas required >50 ms for activation. This probably reflects the more limited contacts between graft and host, as well as slower propagation within the immature graft myocardium.

These intravital imaging studies are, to our knowledge, the first direct demonstration that human cardiomyocytes can integrate and contract synchronously with host myocardium. Although additional paracrine mechanisms cannot be excluded, the demonstration of electromechanically coupled grafts in injured hearts supports the idea that hESC-CMs can improve mechanical function by creating new force-generating units, a sine qua non for heart regeneration. However, hESC-CM grafts in injured hearts were not always fully integrated, implying that enhancing their integration may further benefit contractile function. The model developed here represents a reasonably high-throughput platform to test strategies to improve host–graft integration (for example, tissue engineering, attenuating graft cell death and reducing fibrosis).

Our study also provides reassurance about the arrhythmogenic risk of cardiac repair with immature stem-cell-derived cardiomyocytes. Consistent with prior transplantation studies with primary fetal mouse cardiomyocytes[10], we observed an arrhythmia-suppressive effect that was unique to cardiomyocyte grafts and occurred despite incomplete host–graft coupling. Although this is encouraging, before clinical translation of hESC-based therapies, it will be necessary to carry out safety and efficacy studies with longer follow-up durations and in a large animal model.

METHODS SUMMARY

GCaMP3-positive hESCs were generated by ZFN-mediated targeting, following a method described previously[21] (Supplementary Fig. 7), and these transgenic and wild-type hESCs were differentiated into cardiomyocytes, as previously reported[2,20]. Guinea-pigs underwent cryoinjury, immunosuppression with cyclosporine plus methylprednisolone, cell transplantation and physiological monitoring as detailed in the Supplementary Methods and Supplementary Fig. 1. Intravital imaging of GCaMP3-positive hESC-CM grafts was carried out on day 14 or 28 after transplantation, using open chest and *ex vivo* Langendorff preparations. GCaMP3 and RH237 fluorescent signals were acquired with a high-speed camera (Andor iXon 860 EM-CCD) on an epifluorescence stereomicroscope. All procedures complied with regulations of the University of Washington Institutional Animal Care and Use Committee.

Full Methods and any associated references are available in the online version of the paper at www.nature.com/nature.

Received 26 April 2011; accepted 12 June 2012.
Published online 5 August 2012.

1. Caspi, O. *et al.* Transplantation of human embryonic stem cell-derived cardiomyocytes improves myocardial performance in infarcted rat hearts. *J. Am. Coll. Cardiol.* **50,** 1884–1893 (2007).
2. Laflamme, M. A. *et al.* Cardiomyocytes derived from human embryonic stem cells in pro-survival factors enhance function of infarcted rat hearts. *Nature Biotechnol.* **25,** 1015–1024 (2007).
3. van Laake, L. W. *et al.* Human embryonic stem cell-derived cardiomyocytes survive and mature in the mouse heart and transiently improve function after myocardial infarction. *Stem Cell Res.* **1,** 9–24 (2007).
4. Tallini, Y. N. *et al.* Imaging cellular signals in the heart *in vivo*: cardiac expression of the high-signal Ca^{2+} indicator GCaMP2. *Proc. Natl Acad. Sci. USA* **103,** 4753–4758 (2006).
5. Tian, L. *et al.* Imaging neural activity in worms, flies and mice with improved GCaMP calcium indicators. *Nature Methods* **6,** 875–881 (2009).
6. Kehat, I. *et al.* Electromechanical integration of cardiomyocytes derived from human embryonic stem cells. *Nature Biotechnol.* **22,** 1282–1289 (2004).
7. Xue, T. *et al.* Functional integration of electrically active cardiac derivatives from genetically engineered human embryonic stem cells with quiescent recipient ventricular cardiomyocytes: insights into the development of cell-based pacemakers. *Circulation* **111,** 11–20 (2005).
8. Gepstein, L. *et al. In vivo* assessment of the electrophysiological integration and arrhythmogenic risk of myocardial cell transplantation strategies. *Stem Cells* **28,** 2151–2161 (2010); erratum **29,** 1475 (2011).
9. Liao, S. Y. *et al.* Proarrhythmic risk of embryonic stem cell-derived cardiomyocyte transplantation in infarcted myocardium. *Heart Rhythm* **7,** 1852–1859 (2010).
10. Roell, W. *et al.* Engraftment of connexin 43-expressing cells prevents post-infarct arrhythmia. *Nature* **450,** 819–824 (2007).
11. Kehat, I. *et al.* Human embryonic stem cells can differentiate into myocytes with structural and functional properties of cardiomyocytes. *J. Clin. Invest.* **108,** 407–414 (2001).
12. He, J. Q., Ma, Y., Lee, Y., Thomson, J. A. & Kamp, T. J. Human embryonic stem cells develop into multiple types of cardiac myocytes: action potential characterization. *Circ. Res.* **93,** 32–39 (2003).
13. Zhu, W. Z. *et al.* Neuregulin/ErbB signaling regulates cardiac subtype specification in differentiating human embryonic stem cells. *Circ. Res.* **107,** 776–786 (2010).
14. Mandel, Y. *et al.* Human embryonic and induced pluripotent stem cell-derived cardiomyocytes exhibit beat rate variability and power-law behavior. *Circulation* **125,** 883–893 (2012).
15. Jonsson, M. K. *et al.* Quantified proarrhythmic potential of selected human embryonic stem cell-derived cardiomyocytes. *Stem Cell Res.* **4,** 189–200 (2010).
16. Chen, H. S., Kim, C. & Mercola, M. Electrophysiological challenges of cell-based myocardial repair. *Circulation* **120,** 2496–2508 (2009).
17. Swoap, S. J., Overton, J. M. & Garber, G. Effect of ambient temperature on cardiovascular parameters in rats and mice: a comparative approach. *Am. J. Physiol. Regul. Integr. Comp. Physiol.* **287,** R391–R396 (2004).
18. Mummery, C. *et al.* Differentiation of human embryonic stem cells to cardiomyocytes: role of coculture with visceral endoderm-like cells. *Circulation* **107,** 2733–2740 (2003).
19. Shiotani, M., Harada, T., Abe, J., Hamada, Y. & Horii, I. Methodological validation of an existing telemetry system for QT evaluation in conscious guinea pigs. *J. Pharmacol. Toxicol. Methods* **55,** 27–34 (2007).
20. Zhu, W. Z., Van Biber, B. & Laflamme, M. A. Methods for the derivation and use of cardiomyocytes from human pluripotent stem cells. *Methods Mol. Biol.* **767,** 419–431 (2011).
21. Hockemeyer, D. *et al.* Efficient targeting of expressed and silent genes in human ESCs and iPSCs using zinc-finger nucleases. *Nature Biotechnol.* **27,** 851–857 (2009).
22. Lieu, D. K. *et al.* Absence of transverse tubules contributes to non-uniform $Ca^{(2+)}$ wavefronts in mouse and human embryonic stem cell-derived cardiomyocytes. *Stem Cells Dev.* **18,** 1493–1500 (2009).
23. Kotlikoff, M. I. Genetically encoded Ca^{2+} indicators: using genetics and molecular design to understand complex physiology. *J. Physiol. (Lond.)* **578,** 55–67 (2007).

Supplementary Information is linked to the online version of the paper at www.nature.com/nature.

Acknowledgements We thank Y. Tallini, L. Linares, B. Johnson and S. Dupras for advice and technical assistance. This work was partly supported by a grant from Geron Corporation (M.A.L.), as well as by US National Institutes of Health grants K08-HL80431 (M.A.L.), R01-HL064387 (M.A.L. and C.E.M.), P01-HL094374 (M.A.L. and C.E.M.), R01-HL084642 (C.E.M.), P01-GM81619 (C.E.M.), U01-HL100405 (M.A.L. and C.E.M.) and R01-HL095828 (N.S. and M.W.K.). Animal experiments were supported in part by the University of Washington's Mouse Metabolic Phenotyping Center, U24-DK076126.

Author Contributions S.F., Y.S., W.-Z.Z., D.F., M.I.K., J.D.G., C.E.M. and M.A.L. designed the study. Y.S. and S.F. led the arrhythmia and calcium imaging experiments, respectively. Y.S. developed and performed the telemetry and programmed electrical stimulation. T.D., J.L.M., A.I., R.H. and M.V. performed telemetric ECG interpretation. The GCaMP3-expressing hESC line was generated by J.G., N.J.P. and B.V.B. V.M., J.K., K.W.M., S.F. and Y.S. carried out and analysed immunohistochemistry experiments. S.F., H.R. and M.A.L. developed and performed guinea-pig-specific *in situ* hybridization. S.F., W.-Z.Z. and D.F. carried out and analysed the GCaMP3 imaging experiments. D.F., M.W.K. and N.S. developed and analysed the voltage mapping experiments. All authors contributed to data analysis and interpretation. Y.S. created the figures with the assistance of S.F., W.-Z.Z., K.W.M. and D.F. C.E.M. and M.A.L. wrote the manuscript.

Author Information Reprints and permissions information is available at www.nature.com/reprints. The authors declare competing financial interests: details are available in the online version of the paper. Readers are welcome to comment on the online version of this article at www.nature.com/nature. Correspondence and requests for materials should be addressed to M.A.L. (laflamme@u.washington.edu) or C.E.M. (murry@uw.edu).

©2012 **Macmillan Publishers Limited. All rights reserved**

METHODS

Cell preparation. Undifferentiated H7 hESCs[24] were expanded using either mouse embryonic fibroblast-conditioned medium (MEF-CM)[25] or a defined medium supplemented with basic fibroblast growth factor and transforming growth factor β1 (R&D Systems)[26]. hESCs were then differentiated into cardiomyocytes using our previously reported directed differentiation protocol that involves the serial application of activin A and bone morphogenetic protein 4 (BMP4, R&D) under defined, serum-free, monolayer culture conditions[2,13,20]. Non-cardiac control cells were generated by subjecting hESCs to the same protocol but without the addition of activin A and BMP4. See Supplementary Fig. 2 for additional immunophenotypic information regarding the two cell preparations employed.

Human ESC-CMs and non-cardiac hESC derivatives were collected and cryopreserved after 16 to 18 days under differentiating conditions. One day before collection, cells were subjected to a pro-survival protocol, previously shown to enhance engraftment after transplantation[2]. In brief, cultures were heat-shocked with a 30-min exposure to 43 °C medium, followed by RPMI-B27 medium supplemented with IGF1 (100 ng ml^{-1}, Peprotech) and cyclosporine A (0.2 μM, Sandimmune, Novartis). One day later, cultures were collected with 0.25% trypsin per 0.5 mM EDTA (Invitrogen) and cryopreserved as described previously[27].

Immediately before transplantation, cells were thawed at 37 °C, washed with RPMI, and suspended in a 150-μl volume (per animal) of pro-survival cocktail (PSC)[2], which consisted of 50% (v/v) growth factor–reduced Matrigel, supplemented with ZVAD (100 mM, benzyloxycarbonyl-Val-Ala-Asp(O-methyl)-fluoromethyl ketone, Calbiochem), Bcl-XL BH4 (cell-permeant TAT peptide, 50 nM, Calbiochem), cyclosporine A (200 nM, Wako), IGF1 (100 ng ml^{-1}, Peprotech) and pinacidil (50 mM, Sigma).

Surgical procedures. For cardiac cryoinjury and ECG transmitter placement, male guinea-pigs (650–750 g, Charles River) were anaesthetized with an intraperitoneal injection of 50 mg kg^{-1} ketamine and 2 mg kg^{-1} xylazine. The skin was shaved and sterilized, a small incision was made in the right flank and the transmitter (PhysioTel model CA-F40, DSI) was inserted in a subcutaneous pocket. The positive and negative leads were then tunnelled subcutaneously to the left fifth intercostal space and the upper sternal midline, respectively. The animal was then intubated, mechanically ventilated and anaesthetized with 1.5% isoflurane. The heart was exposed by a left thoracotomy, the pericardium was opened and a 10-mm-diameter aluminium cryoprobe, pre-cooled with liquid nitrogen, was applied to the left ventricular free wall 4 times for 30 s each. At the end of the surgery, all animals received 0.025% (v/v) topical bupivicaine at the wound site, as well as 0.05 mg kg^{-1} intraperitoneal buprenorphine for analgesia.

From day −2 to day +28 relative to cell transplantation, animals were treated with an immunosuppressive regimen of methylprednisolone (2 mg kg^{-1} per day, intraperitoneal) and cyclosporine A (15 mg kg^{-1} per day, subcutaneous, for 7 days; thereafter reduced to 7.5 mg kg^{-1} per day). The trough level of blood cyclosporine was measured on day +28 at 838 ± 64 μg l^{-1}. Cell transplantation was carried out using a repeat thoracotomy and injecting the total bolus of cells into three separate injection sites, that is, the central cryolesion and the flanking lateral border zones.

Echocardiography. On days −2 and +28 relative to cell transplantation, animals were lightly anaesthetized with inhaled 1.5% isoflurane, and then their left-ventricular end-diastolic dimension (LVEDD), left-ventricular end-systolic dimension (LVESD) and heart rate were measured by transthoracic echocardiography (GE Vivid 7) with a 10-MHz paediatric transducer. Fractional shortening (FS) was calculated using this equation: FS = 100 × ((LVEDD – LVESD) / LVEDD). All echocardiographic scans and analyses were performed by an operator who was blind to the experimental conditions.

Telemetric electrocardiography. ECG recordings were acquired from conscious, freely mobile animals using a Dataquest ART telemetry system (DSI)[19,28]. All recordings were obtained at the same time of day (evening) for 6 h (3 h in the light, 3 h in the dark) during a period in which the animals' living quarters were undisturbed. Recordings were obtained from cryoinjured recipients of hESC-CMs, non-CMs or PSC only, on days 1, 6 and 9 after injury and days 1, 3, 7, 10, 14, 17, 21, 24 and 27 after transplantation. All ECG traces were evaluated manually by a cardiologist who was blind to the experimental conditions. The cardiologist determined the total number and frequency of events including single and multiform PVCs, as well as non-sustained and sustained ventricular tachycardia . In accordance with Lambeth convention guidelines[29], ventricular tachycardia was defined as a run of 4 or more PVCs, and sustained ventricular tachycardia was defined as a fast ventricular rhythm of more than 15 beats.

Programmed electrical stimulation. PES studies were performed on day +28 after transplantation, using methods modified from a previous study[30]. In brief, each animal was mechanically ventilated, anaesthetized with 2% isoflurane, and outfitted for standard surface ECG recordings (ADInstruments). A midline incision was made in the epigastric region, and a custom-designed bipolar stimulating electrode (FHC) was inserted through the diaphragm into direct contact with the cardiac apex. PES studies were then carried out using a stimulator generator (STG-1000, MultiChannel Systems) with the pulse output set at twice the capture threshold and the pulse width at 1 ms. We used standard clinical PES protocols, including the application of single, double and triple extra stimuli after a train of 8 conditioning stimuli at a 150-ms cycle length. To determine the ventricular effective refractory period (VERP), a first extra stimulus (S2) was applied with the S1–S2 interval decreased in 5-ms increments from 150 ms until the occurrence of loss of capture. The heart was then challenged three times with the train of eight followed by the single extra stimulus (with the S1–S2 interval set at VERP + 10 ms). If no ventricular tachycardia was induced, this procedure was repeated to apply three challenges with double and, if necessary, triple extra stimuli. In each case, the coupling interval between the final two pulses was set at the VERP for the last extra stimulus + 10 ms. Ventricular tachycardia was only induced in cryoinjured animals with the application of a triple extra stimulus. Notably, ventricular-tachycardia induction by PES was strongly associated with a history of spontaneous ventricular tachycardia during the final day of telemetry monitoring ($P < 0.001$, McNemar's test).

Generation of the GCaMP reporter hESC line. A transgene encoding for the constitutive expression of GCaMP3 was inserted into the AAVS1 locus in H7 hESCs, using methods adapted from a previous study[21] (see Supplementary Fig. 7). In brief, the right and left arms of an AAVS1-specific ZFN were *de novo* synthesized (Genscript) and cloned into a single polycistronic plasmid in which the expression of each was driven by an independent human PGK promoter. A second polycistronic vector was generated in which (approximately 800-bp) homology arms flanking the AAVS1 ZFN cut site (pZDonor, Sigma Aldrich) surrounded a 5.1-kb insert with two elements: a cassette in which the CAG promoter drives expression of GCaMP3 (ref. 5) (Addgene, plasmid #22692) and a second cassette encoding for PGK-driven expression of neomycin resistance.

AAVS1 ZFN (5-μg) and AAVS1 CAG GCaMP3 targeting vector (40-μg) plasmids were co-electroporated (Lonza, Nucleofection system) into H7 hESCs cultured in MEF-CM supplemented with 10 μM Y-27632. Green fluorescent colonies were isolated and expanded and selected with 40 to 100 μg ml^{-1} G418 (Invitrogen) for 5 to 10 days. GCaMP3 H7 hESCs showed a normal karyotype.

Southern blot analysis. Wild-type and transgenic GCaMP3-positive hESC genomic DNA were digested with the restriction enzyme SphI, run on 1% polyacrylamide gel and transferred to a membrane (BioRad Zeta Probe). The membrane was washed in 2× SSC and dried at 80 °C in a hybridization oven for 2 h, followed by 1 h of pre-hybridization in 50% formamide, 0.12 M NaH_2PO_4, 0.25 M NaCl, 7% SDS, and 1 mM EDTA at 43 °C. A hybridization probe was generated with the following primers: CCTGTTAGGCAGATTCCTTATC (sense), AGATGGTGGA CGAGGAAGGGG (antisense). The probe was labelled with ^{32}P dCTP (Amersham Megaprime DNA labelling system) and hybridized overnight in hybridization buffer at 43 °C. After 24 h, the membrane was washed for 20 min with 2× SSC/0.1% SDS followed by 20 min in 0.1× SSC/0.1% SDS. The membrane was then exposed to autoradiographic film for 3 days. The wild-type band is expected at 6.5 kb, whereas the targeted locus shifts to 2.9 kb.

Imaging of GCaMP3-expresssing grafts. Intravital imaging of hearts with GCaMP3-positive grafts was performed on days 14 and 28 after transplantation using either an open-chest or *ex vivo* preparation. For the open-chest preparation, guinea-pigs were anaesthetized, mechanically ventilated and outfitted for standard surface ECG recordings, as described above. The anterior epicardium was then exposed by a wide thoracotomy and visualized using an epifluorescence stereomicroscope (Nikon, SMZ 1000) equipped with an EXFO X-Cite illumination source. GCaMP3 was excited at 450 to 490 nm and bandpass filtered (500 to 550 nm) before detection by an electron-multiplying, charge-coupled device camera (Andor iXon 860 EM-CCD) controlled by Andor Solis software. GCaMP3 image acquisition was typically at 80 to 140 frames per second (f.p.s.). Signals from the charge-coupled device (CCD) camera and the surface ECG were fed through a computer for digital storage and off-line analysis using Andor software and custom Matlab scripts (MathWorks).

Some engrafted hearts were also imaged *ex vivo* after mechanical arrest to eliminate motion artefacts. For these experiments, the heart was collected, rapidly mounted on a gravity-fed Langendorff apparatus and then perfused with modified Tyrode solution at 37 °C. The epicardial GCaMP3 signal was then recorded before and after supplementation of the perfusate with an excitation-contraction uncoupler, either 2,3-butanedione monoxime (BDM, 20 mM)[31,32] or blebbistatin (10 μM)[33]. The utility of blebbistatin was limited by its substantial blue-green fluorescence[34], which interfered with the acquisition of the GCaMP3 signal, so BDM was used in experiments except where otherwise indicated (see Supplementary Table 3). All quantitative comparisons were carried out using hearts treated with the same uncoupler. The electrical activity of the isolated heart was continuously monitored by placing positive and negative ECG leads at the base of the right ventricle and left ventricular apex, respectively. Although most

©2012 Macmillan Publishers Limited. All rights reserved

imaging experiments were carried out under spontaneous conditions, a subset of hearts was also imaged during external pacing at rates from 3 to 6 Hz (ML866 PowerLab 430 Data Acquisition System). Experiments involving pacing at rates of greater than 5 Hz were sometimes limited by the occurrence of irreversible tachyarrhythmias.

In a subset of hearts, GCaMP3 activation maps were generated by determining the interval between a pacing stimulus (or the host QRS complex) and the initial rise in GCaMP3 fluorescence. For this analysis, raw data from the green fluorescence and ECG channels were read into a custom Matlab script for analysis. The GCaMP3 fluorescent signal was median filtered in time to reduce noise, smoothed with a spatial conical filter, and background subtracted. Regions of graft were user defined and then analysed to determine the relative GCaMP3 activation time on a per-pixel basis. Relative GCaMP3 activation times for each pixel were then averaged over several stimuli to generate GCaMP3 activation maps.

Voltage-mapping studies. The preceding imaging system and experimental preparation was also used in optical mapping studies with the potentiometric dye RH237. RH237 was selected as our dye of choice, given our past experience with this indicator and its reasonable spectral separation from GCaMP3. When examined in the same heart, GCaMP3 (green-channel) and RH237 (red-channel) fluorescent signals were acquired consecutively by an exchange of filter cubes, not simultaneously.

In brief, cryoinjured hearts with or without 28-day-old GCaMP3-positive hESC-CM grafts were mounted on a Langendorff apparatus and loaded with RH237 (40 μM) by a bolus injection (in 10 ml buffer) into the aorta. After an initial stabilization period, RH237-stained hearts were then imaged during both spontaneous and paced rhythms. RH237 was excited at 520 to 550 nm, and emitted light was long-pass filtered (670 nm) before detection at 500 f.p.s. using the high-speed EM-CCD system mentioned above. The resultant fluorescent signals were analysed as described previously[35–37]. In brief, background fluorescence was subtracted and the signal at each pixel was smoothed using a median temporal filter and a spatial cone filter. The signal at each pixel was then scaled as a percentage of the maximum optical action potential amplitude for all the pixels. Although not simultaneously acquired, RH237 and GCaMP3 signals could be partially correlated in a subset of paced hearts by aligning repetitive signals relative to the stimulating electrode.

Histology. Histological studies were carried out as detailed previously by our group[2,38,39]. For immunohistochemistry, we used the primary antibodies detailed in Supplementary Table 4, then either fluorescent secondary antibodies (Alexa-conjugated, species-specific antibodies from Molecular Probes) or the avidin-biotin reaction followed by chromogenic detection (ABC kits from Vector Labs). The guinea-pig-specific *in situ* hybridization probe was generated using methods adapted from another study[40]. In brief, guinea-pig genomic DNA was amplified using PCR primers reported previously[40] (sense: 5′-CTCCTGTCCT GCATCCACT-3′; antisense: 5′-GGATATGAGAGACAGTGGTG-3′). The resultant 345-bp band was excised and then amplified in a second round of PCR doped with digoxigenin-11-dUTP. Subsequent *in situ* hybridization with this digoxigenin-labelled guinea-pig-specific probe was carried out using methods detailed previously for the human-specific pan-centromeric probe[2]. The hybridized probe was detected using a peroxidase-conjugated anti-digoxigenin antibody (Roche), followed either by a chromogenic peroxidase substrate or fluorescent tyramide signal amplification (Molecular Probes).

Statistical analysis. All data were analysed in a blind manner, with the identifier code revealed only after the analysis was completed. All values were expressed as mean ± standard error. Statistical analyses were performed using PASW Statistics 18, Graphpad Prism and SAS software, with the threshold for significance level set at $P < 0.05$. Echocardiographic outcomes were analysed using an analysis of variance (ANOVA), then by post-hoc comparisons between groups by Tukey HSD, and time-course changes were analysed using paired *t*-test analysis of means. For comparisons of the fraction of animals showing spontaneous or induced arrhythmias, we used a two-sided Fisher's exact test. The incidence of spontaneous arrhythmias was analysed using a Poisson regression model to adjust for repeated measures and the effect of time. This approach was used to calculate the ratio of the observed frequencies of recurrence for the two groups and the 95% confidence interval. We used the McNemar's test for correlated proportions to test for an association between induced ventricular tachycardia and spontaneous ventricular tachycardia either on the final day of monitoring or throughout days 3 to 28 after the transplantation monitoring period. To test for synchrony between GCaMP3 fluorescence and ECG signals, intervals were compared using ANOVA and then a post-hoc Dunnett's test.

24. Thomson, J. A. *et al.* Embryonic stem cell lines derived from human blastocysts. *Science* **282,** 1145–1147 (1998).
25. Xu, C. *et al.* Feeder-free growth of undifferentiated human embryonic stem cells. *Nature Biotechnol.* **19,** 971–974 (2001).
26. Li, Y., Powell, S., Brunette, E., Lebkowski, J. & Mandalam, R. Expansion of human embryonic stem cells in defined serum-free medium devoid of animal-derived products. *Biotechnol. Bioeng.* **91,** 688–698 (2005).
27. Xu, C. *et al.* Efficient generation and cryopreservation of cardiomyocytes derived from human embryonic stem cells. *Regen. Med.* **6,** 53–66 (2011).
28. Shiotani, M. *et al.* Practical application of guinea pig telemetry system for QT evaluation. *J. Toxicol. Sci.* **30,** 239–247 (2005).
29. Walker, M. J. *et al.* The Lambeth Conventions: guidelines for the study of arrhythmias in ischaemia infarction, and reperfusion. *Cardiovasc. Res.* **22,** 447–455 (1988).
30. Gutstein, D. E., Danik, S. B., Sereysky, J. B., Morley, G. E. & Fishman, G. I. Subdiaphragmatic murine electrophysiological studies: sequential determination of ventricular refractoriness and arrhythmia induction. *Am. J. Physiol. Heart Circ. Physiol.* **285,** H1091–H1096 (2003).
31. Biermann, M. *et al.* Differential effects of cytochalasin D and 2,3 butanedione monoxime on isometric twitch force and transmembrane action potential in isolated ventricular muscle: implications for optical measurements of cardiac repolarization. *J. Cardiovasc. Electrophysiol.* **9,** 1348–1357 (1998).
32. Laurita, K. R. & Singal, A. Mapping action potentials and calcium transients simultaneously from the intact heart. *Am. J. Physiol. Heart Circ. Physiol.* **280,** H2053–H2060 (2001).
33. Fedorov, V. V. *et al.* Application of blebbistatin as an excitation-contraction uncoupler for electrophysiologic study of rat and rabbit hearts. *Heart Rhythm* **4,** 619–626 (2007).
34. Kolega, J. Phototoxicity and photoinactivation of blebbistatin in UV and visible light. *Biochem. Biophys. Res. Commun.* **320,** 1020–1025 (2004).
35. Asfour, H., Swift, L. M., Sarvazyan, N., Doroslovacki, M. & Kay, M. W. Signal decomposition of transmembrane voltage-sensitive dye fluorescence using a multiresolution wavelet analysis. *IEEE Trans. Biomed. Eng.* **58,** 2083–2093 (2011).
36. Kay, M., Swift, L., Martell, B., Arutunyan, A. & Sarvazyan, N. Locations of ectopic beats coincide with spatial gradients of NADH in a regional model of low-flow reperfusion. *Am. J. Physiol. Heart Circ. Physiol.* **294,** H2400–H2405 (2008).
37. Swift, L. *et al.* Controlled regional hypoperfusion in Langendorff heart preparations. *Physiol. Meas.* **29,** 269–279 (2008).
38. Fernandes, S. *et al.* Human embryonic stem cell-derived cardiomyocytes engraft but do not alter cardiac remodeling after chronic infarction in rats. *J. Mol. Cell. Cardiol.* **49,** 941–949 (2010).
39. Laflamme, M. A. *et al.* Formation of human myocardium in the rat heart from human embryonic stem cells. *Am. J. Pathol.* **167,** 663–671 (2005).
40. Kuznetsov, S. A. *et al.* Circulating skeletal stem cells. *J. Cell Biol.* **153,** 1133–1140 (2001).

©2012 **Macmillan Publishers Limited. All rights reserved**